Laser Speckle Techniques for *in situ*-Monitoring of Erosion and Redeposition at Inner Walls in Large Experimental Fusion Devices

A.W. Koch *), M. Ruprecht *) and R. Wilhelm

*) LMT Lehrstuhl für Meßtechnik, Universität des Saarlandes

IPP 4/271 November 1995

MAX-PLANCK-INSTITUT FÜR PLASMAPHYSIK

85748 GARCHING BEI MÜNCHEN

MAX-PLANCK-INSTITUT FÜR PLASMAPHYSIK
GARCHING BEI MÜNCHEN

Laser Speckle Techniques for *in situ*-Monitoring of Erosion and Redeposition at Inner Walls in Large Experimental Fusion Devices

A.W. Koch *), M. Ruprecht *) and R. Wilhelm

*) LMT Lehrstuhl für Meßtechnik, Universität des Saarlandes

IPP 4/271 November 1995

Die nachstehende Arbeit wurde im Rahmen des Vertrages zwischen dem Max-Planck-Institut für Plasmaphysik und der Europäischen Atomgemeinschaft über die Zusammenarbeit auf dem Gebiet der Plasmaphysik durchgeführt.

LASER SPECKLE TECHNIQUES FOR IN-SITU MONITORING OF EROSION AND REDEPOSITION AT INNER WALLS IN LARGE EXPERIMENTAL FUSION DEVICES

A.W. Koch *), M. Ruprecht *) and R. Wilhelm

*) LMT Lehrstuhl für Meßtechnik, Universität Saarbrücken

Contents

Abstract

A method is described which permits non-intrusive two-dimensional optical measurements of surfaces of inner walls of experimental fusion devices. The technique is based on "speckle interferometry" [1-3]. The surfaces to be examined are rough in the order of the wavelength. In the present feasibility study a multi-wavelength CW laser, a pulsed laser system and a MCP-intensified CCD camera are used. The superposition of image intensities taken at two different wavelengths or two different angles of incidence gives an adjustable resolution in the micrometre to millimetre range. First results of reproducible measurements of fusion-relevant surfaces are presented.

1 Introduction

One of the crucial physics issues to be faced in a fusion reactor such as the proposed International Thermonuclear Experimental Reactor (ITER) concerns the amount of power incident at the divertor strike point [4]. Peak power fluxes onto the plasma-facing surfaces during normal operation are expected to be 5-30 MW/m^2, and much higher during transient events such as disruptions. Extrapolation of the results from existing tokamaks would suggest that at these power levels the rate of erosion by sputtering on the target plates would be unacceptably high. However, if the divertor operates in a high-recycling regime (i.e. at high target density), local redeposition of the eroded material [5] may reduce the net erosion to an acceptable level [4]. It is of paramount importance that this redeposition effect is confirmed in an experimental fusion device such as ITER or W7X.

In a fusion reactor, plasma facing components are eroded by a large amount. Calculations of reactor-relevant heat and particle fluxes require redeposition of 98 to 99 % of the eroded material in order to obtain reasonable lifetimes of the plasma facing components. The ultimate aim is the adjustment of plasma boundary conditions to minimize the wall load.

The aim of the technique presented here is the detailed in-situ investigation of plasma facing components. Long term integration over many plasma shots and artificial surface preparation have to be avoided. Many attempts are being made to measure the erosion/redeposition structures by probes [6] applied internally in the tokamak or by studying the erosion of thin transparent films [7]. Probes which are applied ex-situ, after the removal of a specific target plate only measure an integral value of a series of plasma shots with different plasma parameters.

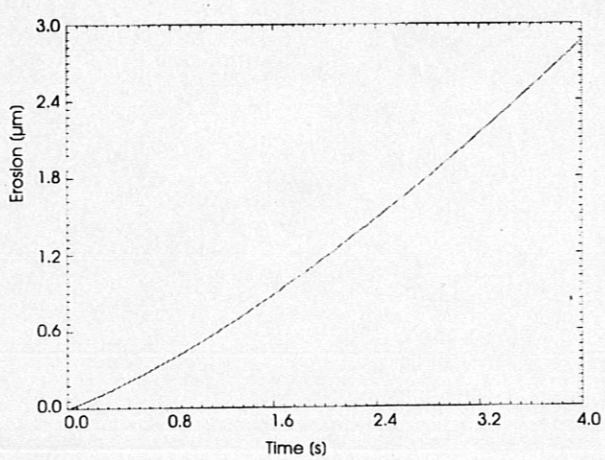

Figure 1-1: Erosion of Be-tiles during plasma exposure [8].

The purpose of the present study is to demonstrate the capability of an optical method which is based on the observation of "speckles" and which provides an in situ means for a direct measurement of surface structures in the micrometre range. It has been turned [8] out that a typical erosion for JET is in the range of some micrometres as shown in Fig.1.1. The method which is proposed and tested is based on speckle techniques. Here, a beam of coherent light is reflected from a surface with a roughness equal or greater than the optical wavelength. The light is reflected and diffracted by the rough surface and may be detected in specular or non-specular directions (Fig. 1.2). By the superposition of the object beam with a reference beam the phase information of the surface signal can be extracted. The phase information gives the surface structure of the illuminated surface. The result of the measurement is a roughness value and respectively a contour-line-plot of changes in surface topology. The changes between subsequent plasma shots are of particular interest for the investigation of target plate erosion/redeposition in experimental fusion devices.

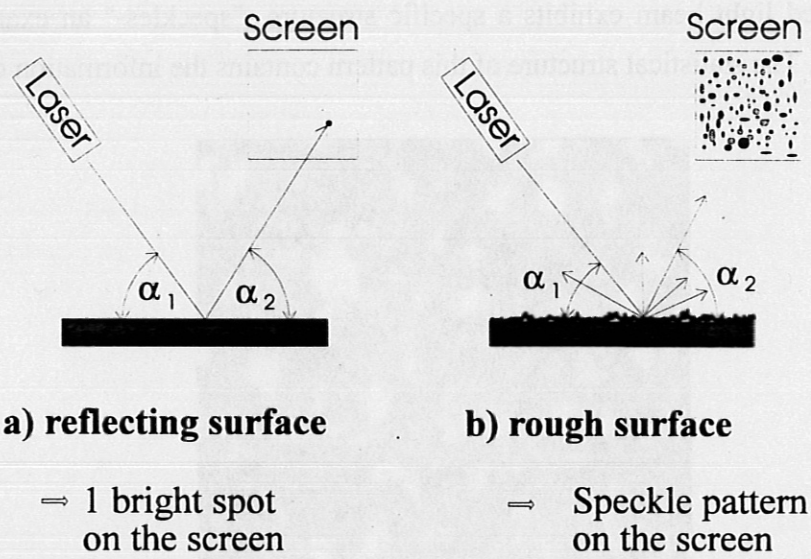

Figure 1-2: Light intensity reflected from a surface being smooth (a) or rough (b).

2 Principle of Measurement

2.1 Speckle size

In contrast to thickness measurements of thin transparent films [9] the intensity pattern of light reflected and diffracted by rough surfaces is rather complicated (Fig. 1.2). Due to interference effects the detected light beam exhibits a specific structure -"speckles-" an example of which is shown in Fig. 2.1. The statistical structure of this pattern contains the information on the phase

Figure 2-1: Typical speckle pattern obtained by reflection and diffraction of light by a rough surface, detected by a CCD camera

change of the incident (coherent) light. To demonstrate this fact, the difference between a specular and a speckled reflection is shown in Fig. 1.2. A surface area of width w_0 is illuminated by an incoming laser beam. For specular reflection, each surface location G_1 and G_2 corresponds to the respective image points B_1 and B_2 in the image plane. For speckled reflection, however, there is a chance of interference between the rays originating from points G_1 and G_2. The resulting intensity variation gives speckles, the size of which is estimated by the following way. B_1' and B_2' are

adjacent points of minimum and maximum intensity, respectively. The size of the illuminated spot is w_0 and the approximate speckle radius is with the target-detector distance

$$Z = z + \Delta d(x,y) \ll w_o \qquad (2.1)$$

where Δx is the geometrical distance of "maximum" to "minimum" intensity on the screen (objective speckle [1]). The speckled reflection results in an interference of beams s_{11}, s_{21} and s_{21}, s_{22} respectively. With $s_{11} = Z$

$$s_{21} \approx Z \cdot \left(1 + \frac{1}{2}\left(\frac{w_o}{Z}\right)^2\right) \qquad (2.2)$$

and thus, the path difference

$$\Delta s_1 = s_{21} - s_{11} = \frac{w_0^2}{2Z} \qquad (2.3)$$

According to Fig 2.2,

$$s_{12} \approx Z \cdot \left(1 + \frac{1}{2}\left(\frac{\Delta x}{Z}\right)^2\right)$$
$$s_{22} \approx Z \cdot \left(1 + \frac{1}{2}\left(\frac{w_o - \Delta x}{Z}\right)^2\right) \qquad (2.4)$$

thus

$$\Delta s_2 = \frac{w_o^2 - 2\Delta x\, w_o}{2Z} \qquad (2.5)$$

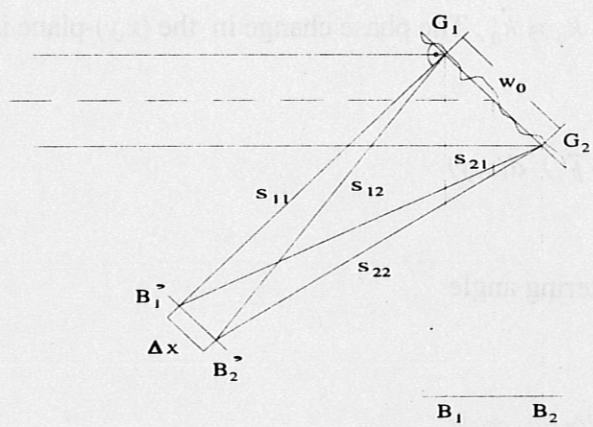

Figure 2.2: Specular and speckled reflection; calculation of speckle size.

If the phase difference $\Delta\Phi_0$ between B_1' and B_2' is π, i.e.

$$\Delta\Phi_0 = \frac{2\pi}{\lambda}(\Delta s_1 - \Delta s_2) = \frac{2\pi}{\lambda}\frac{\Delta x\, w_o}{Z} = \pi \qquad (2.6)$$

where λ is the wavelength of the illuminating light beam, eq. (2.6) is a measure for the average speckle radius. Thus, the size (diametre) of objective speckles [1] is given by

$$\Delta x_{Sp} = \lambda \frac{Z}{w_o} \qquad (2.7)$$

The speckles are then imaged onto the CCD camera by a viewing lens system (subjective speckle). The detection system must be adapted to the average speckle size according to Eq. (2.7), as will be shown in section 3.1.

2.2 Phase shift by surface displacement

As far as the implementation of the speckle technique for fusion wall studies is concerned, an area of typically at least 100 cm^2 has to be illuminated. In order to illustrate the principle of surface structure measurements, Fig. 2.3 shows a part of a target plate of interest before (a) and after (b) erosion. Each surface point is illuminated by the laser and imaged onto the CCD-Detector. Surface erosion causes a point with coordinates (x,y) to move in the direction $\vec{d}(x,y)$. For $|\vec{d}(x,y)| << z_1, z_2$ follows $\vec{k}_0 \approx \vec{k}_0'$. The phase change in the (x,y)-plane is given by

$$\Delta\Phi_s(x,y) = (\vec{k}_o - \vec{k}_s)\cdot\vec{d}(x,y) \qquad (2.8)$$

and, with θ being the scattering angle

$$\Delta\Phi_s(x,y) = \frac{4\pi}{\lambda} d(x,y)\cdot\cos\theta \qquad (2.9)$$

It is evident from the above considerations, that this method of measurement cannot distinguish between surface erosion/ redeposition effects and surface displacement, as pointed out in Fig. 3.1.

In order to retrieve the phase information from the scattered light, the scattered light amplitude

$$\underline{u}_s = \underline{U}_s \cdot \exp(i\Phi_s) \qquad (2.10)$$

with

$$\Phi_s = \Phi_s(d(x, y))$$

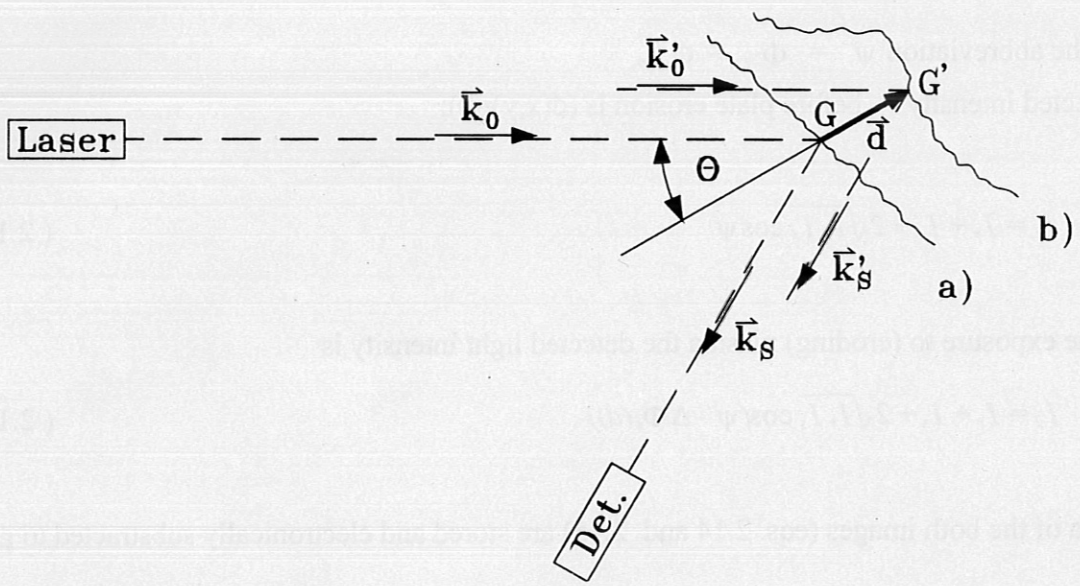

Figure 2.3: Phase shift due to the erosion of a target plate; a) before erosion, b) after erosion.

and

$$I_s = \underline{u}_s \cdot \underline{u}_s^*$$

is superposed by a reference wave

$$\underline{u}_r = \underline{U}_r \exp(i\Phi_r) \qquad (2.11)$$

with

$$I_r = \underline{u}_r \cdot \underline{u}_r^*$$

The phase of the reference wave Φ_r = const. whereas the phase of the scattered wave is

$$\Phi_s = \Phi_{so} + \Delta\Phi_s(x,y) \qquad (2.12)$$

with Φ_{so} =const. and

$$\Delta\Phi_s(x,y) = \frac{4\cdot\pi}{\lambda}\cdot d(x,y)\cdot\cos\Theta$$

The resulting light intensity incident on the detection system is given by

$$I = |\underline{u}_s + \underline{u}_r|^2 = I_r + I_s + 2\sqrt{I_r I_s}\cos\left(\Phi_r - \Phi_s(d)\right) \qquad (2.13)$$

Using the abbreviation $\psi = \Phi_r - \Phi_{so}$
the detected intensity I_1 before plate erosion is (d(x,y)=0):

$$I_1 = I_r + I_s + 2\sqrt{I_r I_s}\cos\psi \qquad (2.14)$$

After the exposure to (eroding) plasma the detected light intensity is

$$I_2 = I_r + I_s + 2\sqrt{I_r I_s}\cos(\psi - \Delta\Phi_s(d)) \qquad (2.15)$$

The data of the both images (eqs. 2.14 and 2.15) are stored and electronically substracted to give

$$\Delta I = |I_1 - I_2| \propto \left(\sin\left(\frac{\Delta\Phi_s(d)}{2}\right)\right) \qquad (2.16)$$

High spatial frequencies do not contribute to the result of eq.(2.16) because the CCD camera acts as a low pass filter. Eq. (2.16) yields interference fringes as a function of the local position *d(x,y)* on the (eroded) plate.

2.3 Two-wavelength technique

The technique of section 2.2 is not applicable to erosion/redeposition measurements in experimental fusion devices because, in the presence of vibrations and displacements of the target plates subsequent images may not be correlated. A further disadvantage is the fixed fringe resolution. To overcome these problems a two-wavelength technique is proposed and tested as will be shown in section 4.2 [16].

The technique is based on the simultaneous illumination of the target plate by two laser beams of different wavelengths. The superposition of object and reference beams in an interferometer (see Fig. 4.6) again results in

$$I = |u_r + u_s|^2 = I_r + I_s + 2\cdot\sqrt{I_r \cdot I_s}\cdot\cos(\Phi_r - \Phi_s) \qquad (2.17)$$

with

$$\Phi_s = \Phi_{s0} + \Delta\Phi_s$$

$$\Delta\Phi_s = \frac{2\cdot\pi}{\lambda_i}\cdot d\cdot 2\cdot\cos\theta \;;\; i = 1,2$$

We use an argon ion laser at the two most intense emission lines, i.e. i=1 corresponds to $\lambda_1 = 514.5\ nm$ and i=2 to $\lambda_2 = 488\ nm$. The respective image intensities are

$$I_i = I_r + I_s + 2\cdot\sqrt{I_r \cdot I_s}\cdot\cos(\Phi_{r_i} - \Phi_{so_i} - \frac{4\cdot\pi}{\lambda_i}\cdot d\cdot\cos\theta) \qquad (2.18)$$

$$\Psi_i := \Phi_{r_i} - \Phi_{so_i} \qquad i=1,2$$

assuming equal laser intensity at both wavelengths. Again the image substraction gives

$$\Delta I = |I_1 - I_2| \propto \left|\sin(\frac{\Psi_1 - \Psi_2}{2} + \frac{\pi\cdot d(x,y)}{\Lambda})\right| \qquad (2.19)$$

The parameter Λ is dependant only on the scattering angle and both wavelengths:

$$\Lambda = \frac{\lambda_1\cdot\lambda_2}{2\cdot(\lambda_1 - \lambda_2)\cdot\cos\theta} \qquad (2.20)$$

and is denoted „synthetic wavelength".

Thus a variable fringe resolution is obtained by the appropriate choice of the illuminating wavelengths. Examples for several wavelength combinations permitted by an argon ion laser are depicted in Fig 2.2.

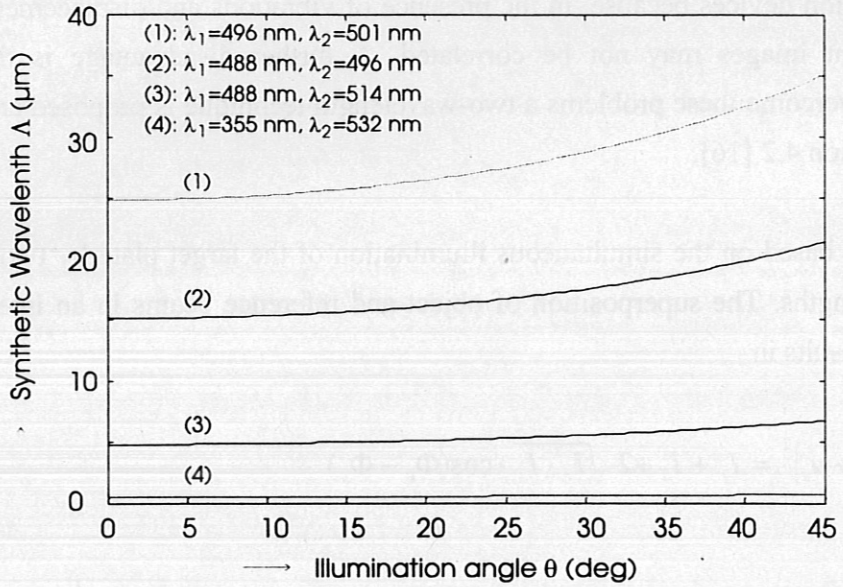

Figure 2-2: Variable fringe resolution. Curves (1)-(3): different wavelength combinations of an argon ion laser, curve (4): Second and third harmonic of a Nd:YAG laser,.

2.4 Two-angle-of-incidence technique

As shown by eq. (2.20) the fringe resolution is not only dependant on the wavelength but also on the angle of incidence of the illuminating laser beam [17]. Following the same procedure as in the previous section the intensities at two *angles* of incidence with i=1,2
eq. (2.18) changes to

$$I_i = I_r + I_s + 2 \cdot \sqrt{I_r \cdot I_s} \cdot \cos(\Psi_i - \frac{4 \cdot \pi}{\lambda} \cdot d \cdot \cos\theta_i) \qquad (2.21)$$

After image substraction

$$\Delta I = |I_1 - I_2| \propto \left| \sin\left(\frac{\Psi_1 - \Psi_2}{2}\right) + \frac{2 \cdot \pi \cdot d}{\lambda} (\cos\theta_1 - \cos\theta_2) \right|$$
$$= \left| \sin\left(\frac{\Psi_1 - \Psi_2}{2} + \frac{\pi \cdot d(x,y)}{\Lambda_\theta}\right) \right| \qquad (2.22)$$

where

$$\Lambda_\theta = \frac{\lambda}{3} \cdot \frac{1}{\cos\theta_1 - \cos\theta_2} \qquad (2.23)$$

In order to avoid speckle decorrelation and/or in-plane sensitive measurements [1] the difference of the angle has to be small, i.e.

$$\Delta\theta = \theta_1 - \theta_2 << \theta_1 \qquad (2.24)$$

The synthetic wavelength may then be written as

$$\Lambda_\theta \approx \frac{\lambda}{2} \cdot \frac{1}{\cos\theta_1 (1 - \cos\Delta\theta)} \qquad (2.25)$$

The adjustable fringe resolution is a function of the parameter Λ_θ.

2.5 Image shearing technique

The most important difference between the two techniques described above and the shearing technique is the absence of a reference beam. The advantage is obvious: Their are no problems with different intensities in both beams and with the coherence length of the used laser light.

For this technique the sample is illuminated by a laser beam without coupling of part of the intensity as reference beam, so that the full intensity of the laser is directed onto the sample. The detection unit consist of a Michelson-interferometer and a CCD-camera (see Fig. 4.13). The scattered light reflected from the surface is split in two parts of equal intensity in the

interferometer. One of the two mirrors, the shear mirror, is tilted with reference to the perpendicular direction. The tilt angle is called shear angle δα. With the shear angle the sensitivity of the measurement system can be adjusted continuously. The images reflected back from the two mirrors of the Michelson interferometer are, as a consequence, sheared against each other. For our first experimental setup, which is equivalent to the speckle shearing interferometer by Leendertz and Butters [11], see section 4.2.3 .

With the shearing technique, as far as it is described here, only relative measurements of changes of the examined surface are possible. We could think about the combination of the shearing technique and the two-wavelength technique to extract absolute information on the surface topology, requiring a more complex experimental setup for fusion devices. With the relative method, we obtain information on the surface change between two measurements. Thus, it is possible to track the change in surface topology during a plasma shot. Through the superposition of the two sheared wavefronts the intensity at one point Q at the screen is the sum of the intensity, reflected from two points P_1 and P_2 at the surface. (Fig. 2.3).

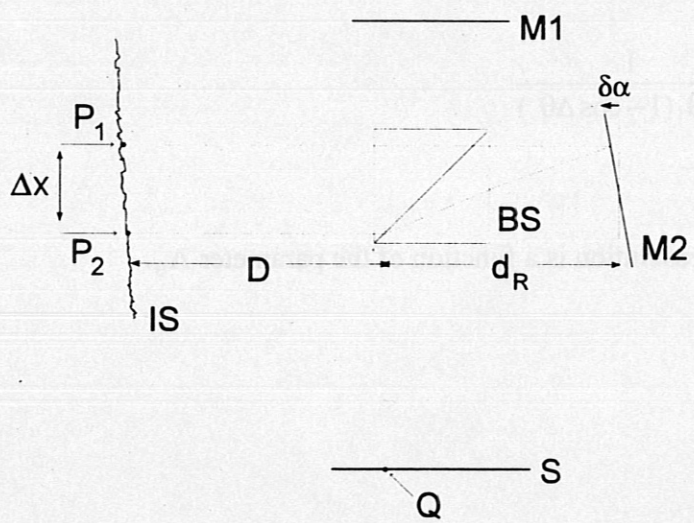

Figure 2-3: Schematic setup of a shearing interferometer. Δx: Distance between P_1 and P_2 at the surface, D: Distance between sample and detection system, d_R: distance between beam splitter (BS) and shearing mirror (M2), δα: shearing angle, M: mirror, IS: illuminated surface, S: screen (or CCD array) P_1, P_2: Two points on the surface, whose images meet at the same point Q on the screen.

The distance Δx of the two points is given by the shear angle δα. For the detection unit in use:

$$\Delta x = (D + d) \cdot \tan(2 \cdot \delta\alpha) \qquad (2.26)$$

with D being the distance between object and detection unit, d the distance between beamsplitter and shearing mirror. The direction of the vectors from P_1 and P_2 is given by the orientation of

the rotation axis of the shearing mirror. For the phase difference $\Delta\Phi$ after deformation, one can write generally:

$$\Delta\Phi = \frac{2\cdot\pi}{\lambda}\cdot(\boldsymbol{n}_0 - \boldsymbol{n}_s)\cdot(\boldsymbol{d} - \boldsymbol{d}') \qquad (2.27)$$

with $\boldsymbol{n}_0$: illumination direction, $\boldsymbol{n}_s$: viewing direction, $\boldsymbol{d}$: displacement of the first point P_1 on the surface, $\boldsymbol{d}'$: displacement of the second point P_2 superimposed with the first point on the image.

In order to elucidate the role of the difference image the term $(\boldsymbol{d} - \boldsymbol{d}')$ is discussed in more detail. For a shift along the x axis, the difference of the out-of-plane deformation in point P_1 and P_2 can be written as:

$$(\boldsymbol{d} - \boldsymbol{d}') \approx \frac{\partial d}{\partial x}\cdot\Delta x_P \qquad (2.28)$$

with d: displacement in one of the points P_1 , P_2 , Δx_P: separation of the images in the image plane due to shearing. The resulting fringe spacing is given by:

$$\Delta = C\cdot\frac{2\cdot\pi}{\partial(\Delta\Phi)/\partial x} = C\cdot\frac{\lambda}{2(\partial^2 d/\partial x^2)\cdot\Delta x_P} \qquad (2.29)$$

with C: constant depending on the illumination and viewing direction. These formulars show that fringes in the difference image are not depending on the surface height, but on the gradient. Thus the fringe spacing depends on the second derivative of the surface displacement.

All the formulars used in this section are only valid for small shear angles. If $\delta\alpha$ is to large, eq. (2.28) is no longer valid. There are two approximations incorporated. The first one is the neglection of terms of higher order. The second one is the approximation of the differential quotient using the derivation. Both are fulfilled for small Δx. If Δx is to large it is very complicated to interpret the results, and for even larger shifts no more fringes will be visible. The maximum Δx allowed depends on the experimental setup. In our case Δx was about 1mm for a detected area of 1 cm^2.

3 Experimental considerations

The implementation of the aforementioned techniques requires careful consideration of many experimental arrangements which cannot be discussed in detail in this report. In the following sections of this chapter we focuse our attention on the detection limits (3.1 and 3.2), the optical system (3.3 and 3.4) and disturbing effects superposing the measurements (3.5).

3.1 Spatial frequency detection limit

Shannon's sampling theorem gives the upper limit of the spatial frequency which can be measured by a detector:

$$f_{\max} < \tfrac{1}{2} \cdot f_{\det} \qquad (3.1)$$

where f_{det} is given by the CCD camera. A typical value can be found from

$$f_{\det} = \frac{n_l}{s} \approx \left. \frac{625}{13\,mm} \right|_{in\ our\ case} \approx 50\,mm^{-1} \qquad (3.2)$$

where n_l is the number of (video) lines and s is the physical size of the CCD chip. The Rayleigh criterion

$$\Delta\Theta = 1.2 \cdot \frac{\lambda}{a} \qquad (3.3)$$

with a being the lens aperture and $\Delta\Theta$ the minimum angle under which two object points can be separated, relates the the speckle size Δx_{sp} to the configuration of the observation optics

$$\Delta x_{Sp} = 2 \cdot \Delta\Theta \cdot b = 2.4 \cdot \lambda \cdot \frac{b}{a} \qquad (3.4)$$

b is the fixed distance between the lens and the CCD chip. Thus, using eq. (3.1) the design formula for the observation optics is obtained

$$f_{\max} \approx (\Delta x_{Sp})^{-1} < \tfrac{1}{2} \cdot f_{\det} \Rightarrow \frac{b}{a} > (1.2 \cdot \lambda \cdot f_{\det})^{-1} \approx 3 \qquad (3.5)$$

for an incident wavelength of 532 nm (Nd:YAG laser with frequency doubler). Eq. (3.5) implies that a certain aperture radius a must not be exceeded. This fact imposes consequences on the amount of the detectable reflected light as shown in the next section.

3.2 Light intensity at the detector

One critical parameter for speckle measurement techniques in large fusion devices is the amount of reflected light. On one hand, a large distance between the surface to be measured and the detector is required, on the other hand low reflecting materials such as graphite tiles are used. The light intensity at the aperture of diameter a of the detector (see Fig. 4.6 b) is [1]:

$$I_a = \rho \cdot g^{-2} \cdot P_0 \qquad (3.6)$$

where P_0 is the laser power incident on the surface under investigation, g is the distance between the surface and the lens, and ρ is the reflection coefficient. The intensity incident on the MCP/CCD camera with an active area A_{det} is

$$I_{\det} = I_a \cdot \frac{\frac{\pi}{4} \cdot a^2}{A_{\det}} \qquad (3.7)$$

Using the abbreviations M for the magnification and F for the F-number of the detection optics

$$M = \sqrt{A_{\det} / A_s}$$
$$F = f_{\det} / a \qquad (3.8)$$

where A_s is the surface area of interest and f_{det} the focal length of the detection optics. In the present case $M \ll 1$ gives

$$F \approx \frac{b}{a} \qquad (3.9)$$

with b being the image width. Thus, using eqs. (3.6-3.9), the detected intensity I_{det} as a function of the optical setup, the incident laser power and the reflection coefficient of the target material is

$$I_{\mathrm{det}} \approx \tfrac{\pi}{4} \cdot \rho \cdot P_0 \cdot \frac{a^2}{M \cdot g^2 \cdot A_s} \approx \tfrac{\pi}{4} \cdot \rho \cdot F^{-2} \cdot \frac{P_0}{A_s} \qquad (3.10)$$

The sampling theorem according to eq. (3.1) and (3.2), gives an estimation for the detectable intensity

$$I_{\mathrm{det}} < \frac{\pi}{4} \cdot \rho \cdot \lambda^2 \cdot f_{\mathrm{det}}{}^2 \cdot \frac{P_0}{A_s} \qquad (3.11)$$

One has to take into account the approximate overall transmissivity of the optical system T = 0.1 and an estimation of the surface parameters $A_s = 0.25\ m^2$ and $\rho = 0.02$. The resulting intensity at the detector using a camera as described in section 3.4 with $f_{det} = 50\ mm^{-1}$ and 640 x 488 pixels and a pulsed Nd:YAG laser as described in section 3.3 with 550mJ per 7 ns- pulse @ λ=532 nm is

$$I_{\mathrm{det}} \leq 3 \cdot 10^{11} \frac{\text{photons}}{\text{pixel} \cdot \text{laser pulse}} \qquad (3.12)$$

which should be sufficient for most applications in fusion research.

3.3 Laser system

The laser system used for the long range measurements is a flash lamp pumped Nd:YAG laser with a frequency doubler. The short pulse duration is achieved by an electro-optical Q-switch. An injection seeder allows locking to a single mode. Some specifications are listed in table 3.3.1

Wavelength	532 nm*), 1064 nm
Max. output energy per pulse	1100 mJ at 1064 nm 550 mJ at 532 nm
Pulse duration (FWHM)	7 ns
Repetiton rate	0.1-10 Hz
	*) used wavelength

Table 3.3.1: Laser data, pulsed system

To apply the two-wavelength technique (see section 2.3) an additional OPO (optical parametrical oscillator) is required which can be pumped by the Nd:YAG laser system and allows to change the wavelength continuously over a wide range of the visible spectrum.

For some previous studies in the laborarory a tunable multi-wavelength argon ion laser was used. The wavelength was changed by turning a prism in the laser resonator. The beam diameter was 50 mm with a telescope optic. The output powers of the used lines are summarized in table 3.3.2.

Wavelength [nm]	Max. output power [mW]
458	110
466	50
473	50
477	250
488	700
497	280
502	100
514	800

Table 3.3.2: Laser data, CW system

3.4 MCP-intensified CCD camera

The main part of the detection system is a CCD camera. For most of the experimental studies in the laboratory a standard CCD camera with about 512x512 pixels and an exposure time of 40 ms is sufficient. For application in long range or field measurements a CCD camera with additional image intensifier (MCP: micro channel plate) is used. There are two essential advantages of this type of camera: Firstly, the sensitivity is much higher, so that measurements on surfaces with a high absorption index, e.g. the graphite tiles of the inner walls of an experimental fusion reactor, are possible. Secondly, it is possible to achieve very short exposure times (down to 5 ns), which eliminates the influence of any vibrations of the measurement object.

The principle of the MCP is based on an array of small multiplier tubes, approx. one for each pixel of the following CCD chip. In front of this array a photo cathode is attached. Inside the tubes the primary electrons are multiplied. A fluorescence layer is placed between the multiplying tubes and the CCD chip. The following table lists some specifications of the used MCP/CCD.

Spectral range	130 nm- 920 nm
Number of pixels	610 (h) x 488 (v)
Coupling MCP-CCD	Lens optic
Sensitivity	5 µ lx
Tube diameter ≈ pixel size	20 µm
Maximum photonic gain of the MCP	10^7
Dynamic range	10^9 : 1
Minimum exposure time	5 ns

Table 3.3.3: Data of detection system

3.5 Deformation and vibration

A critical influence on speckle experiments in fusion devices is briefly addressed in this section: the influence of surface changes not caused by erosion and/or redeposition. The principle of the speckle techniques described in chapter 2 are relative measurements, i.e. absolute distances cannot be obtained. The situation is shown in Fig. 3.1: The technique cannot discriminate between situations b) and c). Nevertheless, the speckle techniques are applicable for a number of measurement problems if reference points are accessible where erosion/redeposition can be excluded. Vibration problems can often be overcome by using short exposure times, as achieved by the MCP/CCD camera described in section 3.4.

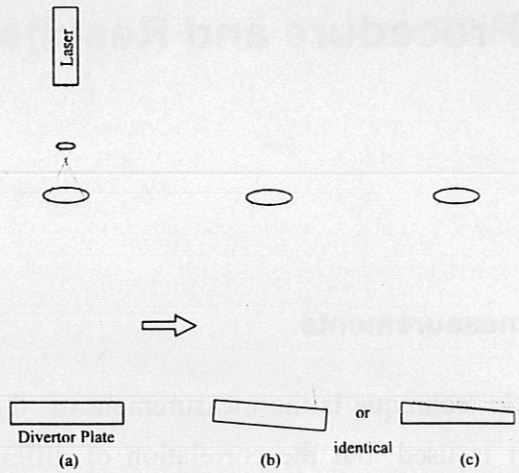

Figure 3-1: Measurement of surface profile. (a): before changes in surface, (b): surface displacement, (c): surface erosion.

In order to qualitatively determine whether erosion/redeposition has occured at all, a method proposed by Salazar et al. [10, 11] is applied. Here, erosion structures become visible in the presence of a target deformation.

4 Measurement Procedure and Results

4.1 Surface roughness measurements

One application of the speckle technique is the measurement of the surface roughness. In this application no interferometer is used, but the correlation of different images taken from the surface. The difference of the images is, according to the different speckle interferometric techniques, the illumination angle (ASC: angular speckle correlation) or the wavelength (SSC: spectral speckle correlation). The method mainly focused on was the ASC, requireing only a standard HeNe laser. For the SSC a tunable multi-wavelength argon-ion laser was used. In Fig. 4.1 a typical experimental setup for ASC is shown.

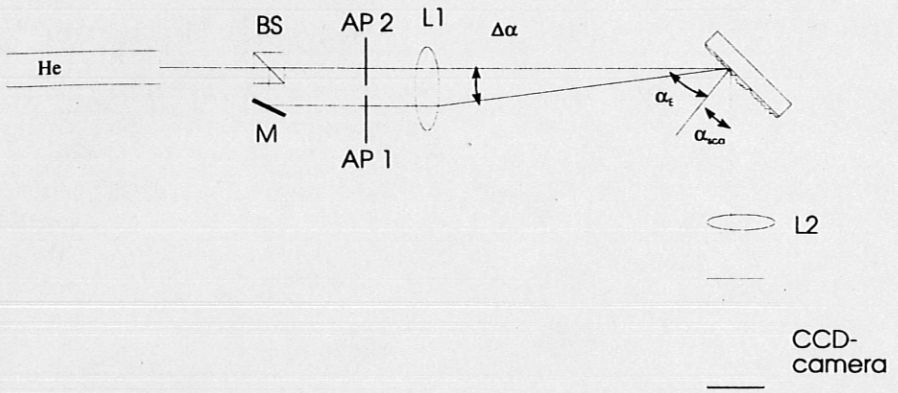

Figure 4-1: Setup for angular speckle correlation (ASC) BS:beam spitter, M: mirror, AP: aperture, L:lens, according to the work of Kirchner [15]

One of the two illuminating beams is blocked to take the first image, for the second image the other beam is blocked. The result of the procedure, containing information on the surface roughness, is the 2D correlation coefficient of the two images. For the ASC it is necessary to shift the second image, before correlating it with the first image, due to the different angles of the illuminating beams. With the CCD camera and the frame grabber card in use, it was possible to obtain images with 512 x 512 pixel resolution for the evaluation of the roughness. The amount of shifting is roughly determined before the images are taken, and it is nearly the same for each pair of images taken with the setup left unchanged. Because it is difficult to correctly obtain the amount of shifting for one pixel, not only one fixed shift is performed, but 50 in each direction.

For all these different positions of the second image the correlation coefficient was calculated. When investigating a speckle pattern, it is important to carefully take into account the optical configuration of the detection unit. In the experiments described here the images were taken in the Fourier plane, i.e the distances between the surface and the image lens and between the image lens and the CCD array correspond to the focal length. The basic formular for the correlation coefficient of two images in the Fourier plane is [12]:

$$K_{12} = \frac{\langle I_1 \cdot I_2 \rangle - \langle I_1 \rangle \cdot \langle I_2 \rangle}{\sigma_1 \cdot \sigma_2} \qquad (4.1)$$

using the intensities and standard deviations of images 1, 2.

For the angular speckle correlation (ASC), the relationship between the surface roughness and the correlation coefficient is given by [12]

$$K_{12} = \exp[-(2 \cdot \sin\alpha \cdot k \cdot \Delta\alpha \cdot \sigma_h)^2] \qquad (4.2)$$

with: α: angle of incidence, $\Delta\alpha$: angle difference between images, k: wave vektor, σ_h : standard deviation of surface height. The coefficient is shown in Fig. 4.2 for three different difference angles $\Delta\alpha$. For the spectral correlation coefficient (SSC), the equivalent formular is:

$$K_{12} = \exp[-(2 \cdot \cos\alpha \cdot \Delta k \cdot \sigma_h)^2] \qquad (4.3)$$

with: Δk: difference between k_1 and k_2, for the different incident wavelength λ.

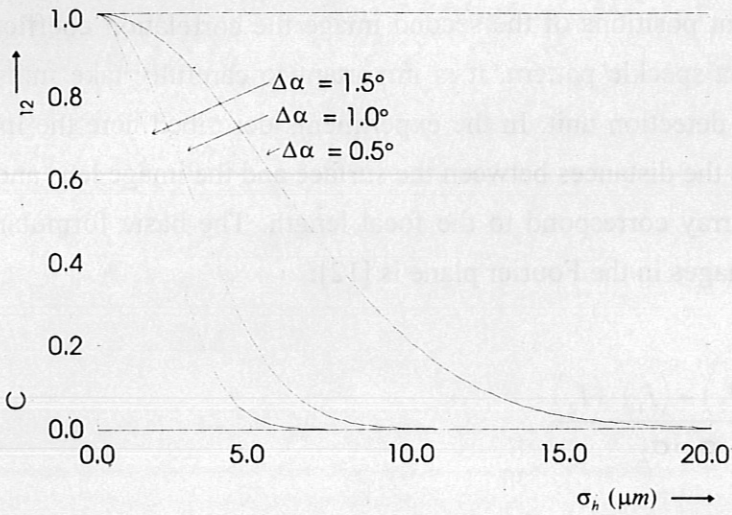

Figure 4-2: Correlation coefficient for ASC in dependence of surface roughness

These formulars are only correct when the speckle pattern is fully developed. This is true for all surfaces with a roughness larger than λ/2. This precondition is met by most of the technical surfaces, whose surface roughnesses are in the range between 0.5 μm and some 10 μm. For the range between a mirror surface and a fully developed speckle pattern, it is possible to get information on the surface roughness by using the contrast of the remaining, not fully developed speckle pattern (see below). For a fully developed speckle pattern the contrast is one, so that it is not possible to use it for roughness evaluation. The following figures show some of the results of the speckle correlation measurements on rough metall samples, alumina and steel, made by Kirchner [15, 23].

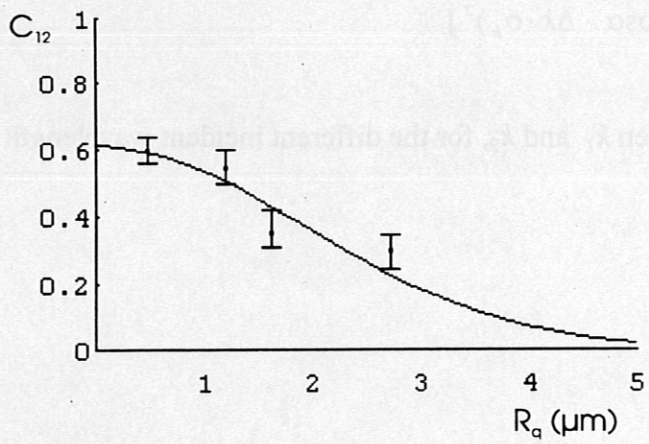

Figure 4-3: ASC measurement at a rough steel surface

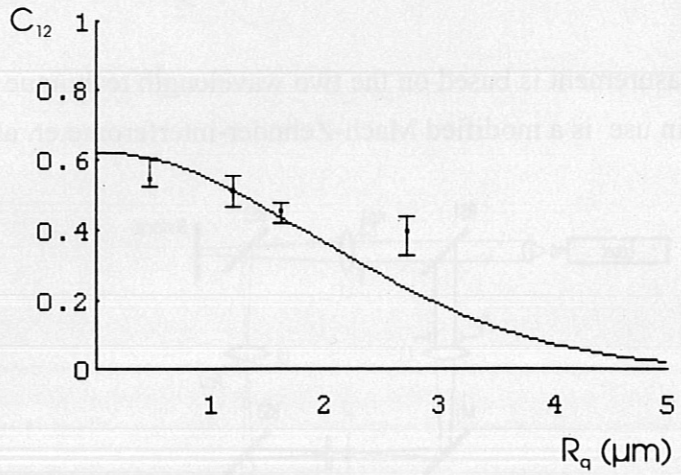

Figure 4-4: SSC measurement at a rough steel surface

Beyond the correlation technique measurements of the contrast of not fully developed speckle patterns were carried out. For these measurements the contrast C_0 was calculated according to formular:

$$C_0 = \frac{\sqrt{\left|\langle I\rangle^2 - \langle I^2\rangle\right|}}{\langle I\rangle} = \frac{\sqrt{\sum I(x,y)^2 - \left(\sum I(x,y)\right)^2}}{\sum I(x,y)} \qquad (4.4)$$

with $I(x,y)$ being the intensity at a single pixel of the image.

The formular is valid for a surface roughness $R_q < \lambda/4$. The result of one measurement is shown in the following table.

Copper sample	Conventional single-line roughness tester Rq [µm]	Contrast C
3	0.277±0.043	0.376±0.014
4	0.259±0.004	0.367±0.009
5	0.274±0.021	0.378±0.014
6	0.303±0.027	0.347±0.023

Table 4.1: Results of contrast measurement of different copper samples.

4.2 Surface contour line measurements

The principle of this measurement is based on the two wavelength technique described in chapter 2.3. The interferometer in use is a modified Mach-Zehnder-interferometer, as shown in Fig. 4.6.

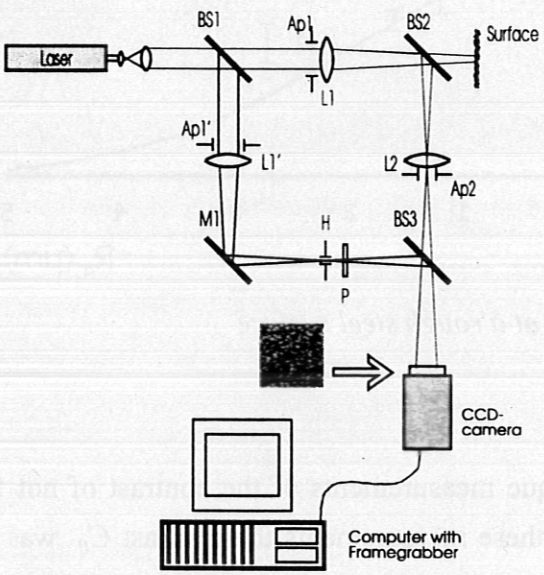

a)

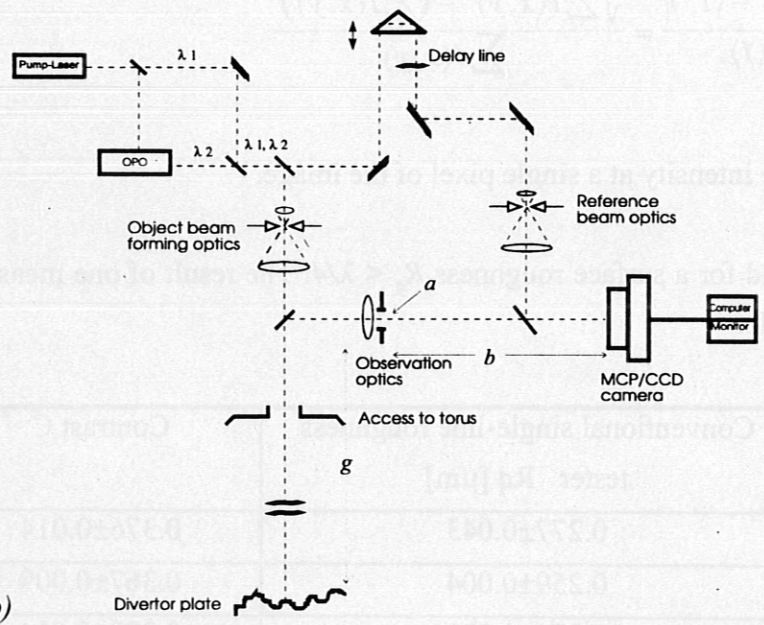

b)

Figure 4-5: Setup for 2λ-speckle interferometry. (a) LMT laboratory setup, (b) proposal for fusion devices. BS: beam splitter, Ap: aperture, M: mirror, L: lens, H: pinhole, OPO: optical parametric oszillator.

According to formular (2.27) the fringe sensitivity is given by the synthetic wavelength Λ. Fig. (2.4) depicts the range which can be realized with the argon ion laser of section 3.3 and the range using the second and third harmonic of a Nd:YAG laser.
For testing this method several measurements were made at a rough alumina plate (*Figure 4.6*). For the two images the 488 nm and the 514 nm lines of an argon ion laser were used.

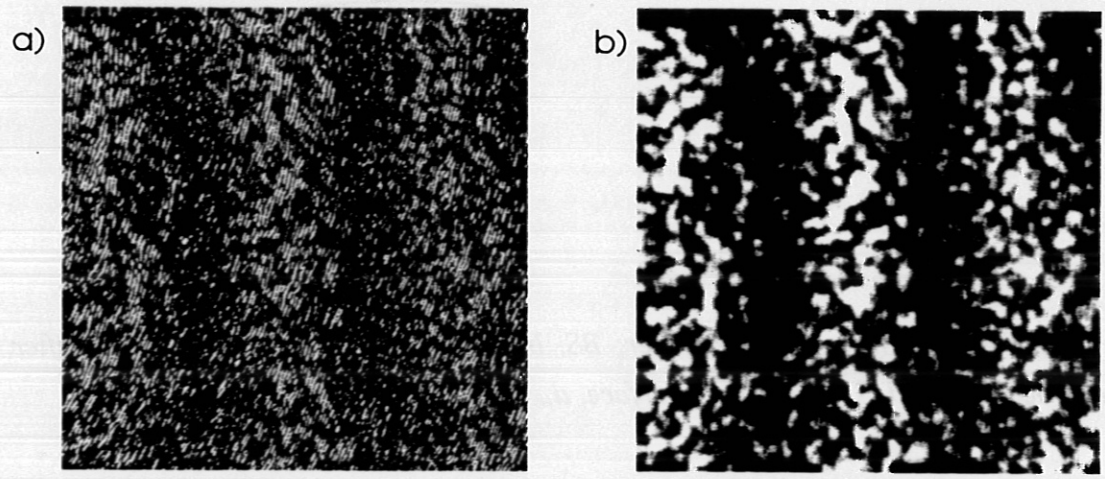

Figure 4-6: 2λ-speckle images of an alumina plate. a): before, b): after image processing.

4.3 Erosion and deformation: qualitative measurements

Most of the experimental results shown in this section were taken with a Twyman-Green-interferometer, as shown in Fig. 4.9. At first the deformation is measured. The procedure for this measurement consists of four steps, (i) one image is taken, (ii) the surface is displaced out-of-plane by some micrometres, (iii) another image is taken and finally (iv) the difference image is calculated. It is necessary to convert the range of intensity values to the gray level intervall [0,255] to monitor the difference image.

A more complicated procedure is required in order to determine the direction of a deformation: phase shifting (see section 2.2). The following figures (4.8-4.9) show the experimental setup, a fringe image without phase shifting and a 3D-plot.

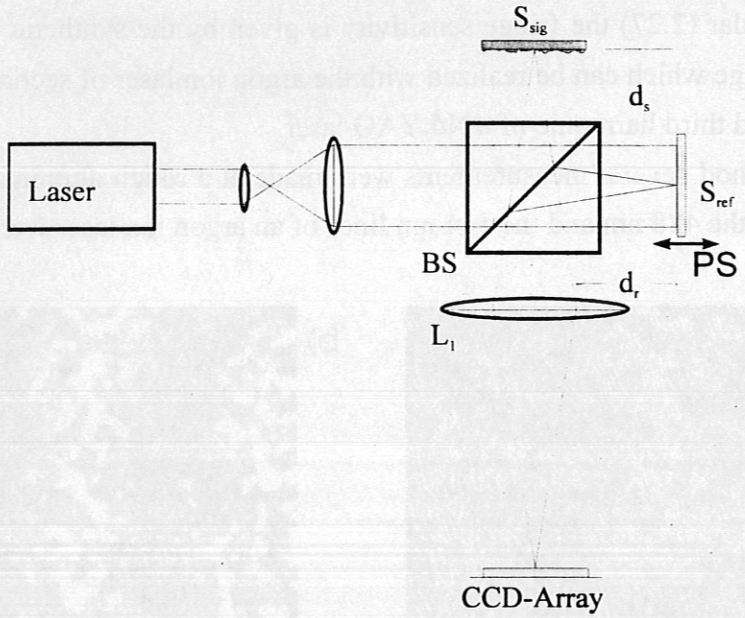

Figure 4-7: Twyman Green interferometer; BS: beam splitter, L: lens, PS: phase shifter, S_{Sig}: surface to be measured, S_{Ref}: reference surface, d_r, d_s: reference- and signaldistance.

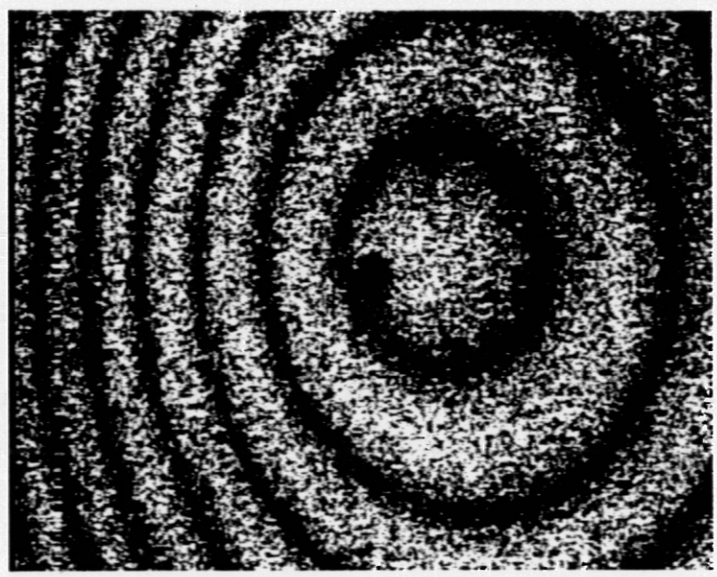

*Figure 4-8: Difference image of an out-of-plane deformation **without** phase shifting. The height distance between two fringes is λ/4 (here: 0.16 µm).*

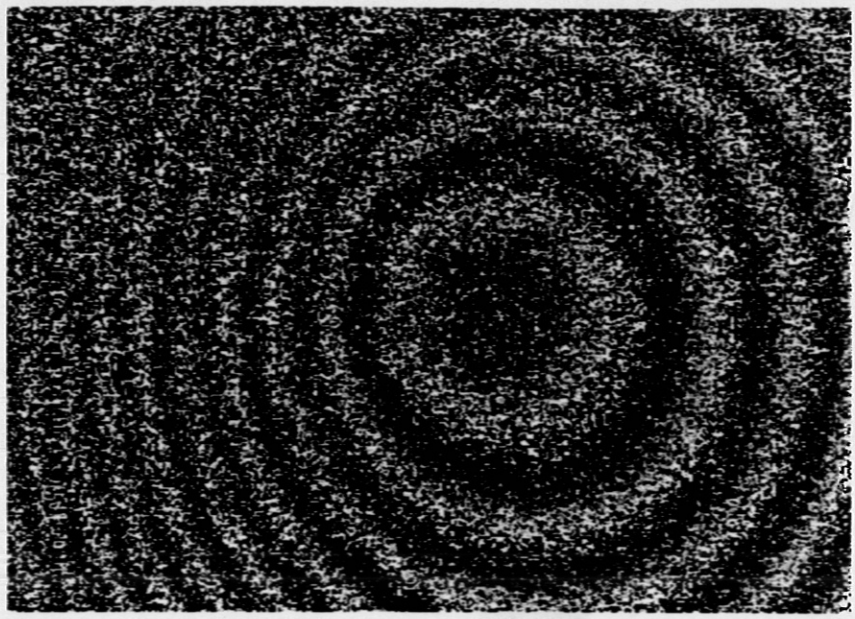

Figure 4-9: Difference image of an out-of-plane deformation ***with*** *phase shifting. The height distance between two fringes is λ/4 (here: 0.16 µm).*

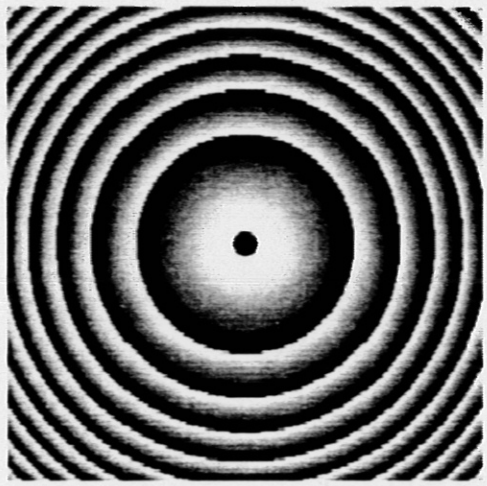

Figure 4-10: Calculated phase shifting image.

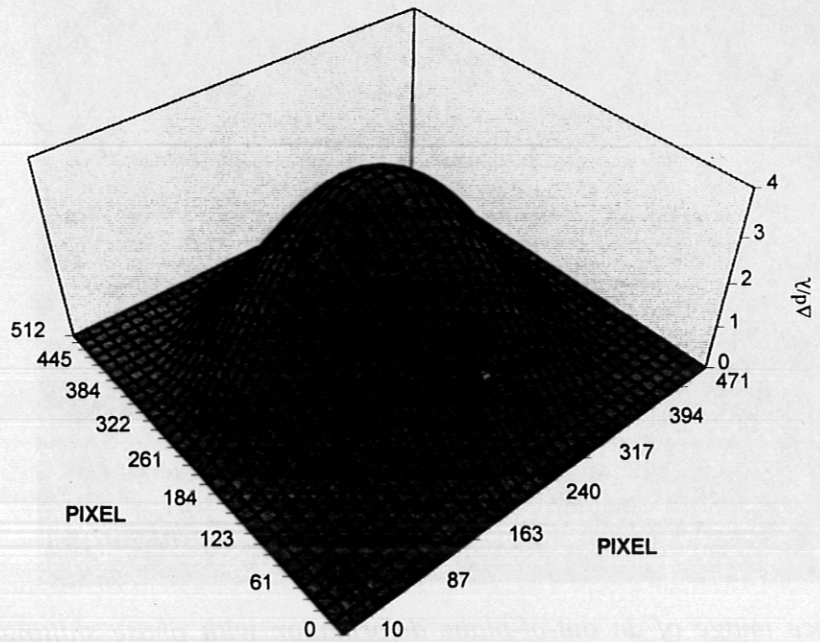

Figure 4-11: 3D-plot of an out-of-plane surface deformation.

Measurements of an equally deformed rough aluminium plate were also made using a shearing interferometer. The setup is shown in Fig. 4.13, the resulting difference image in Fig. 4.14.

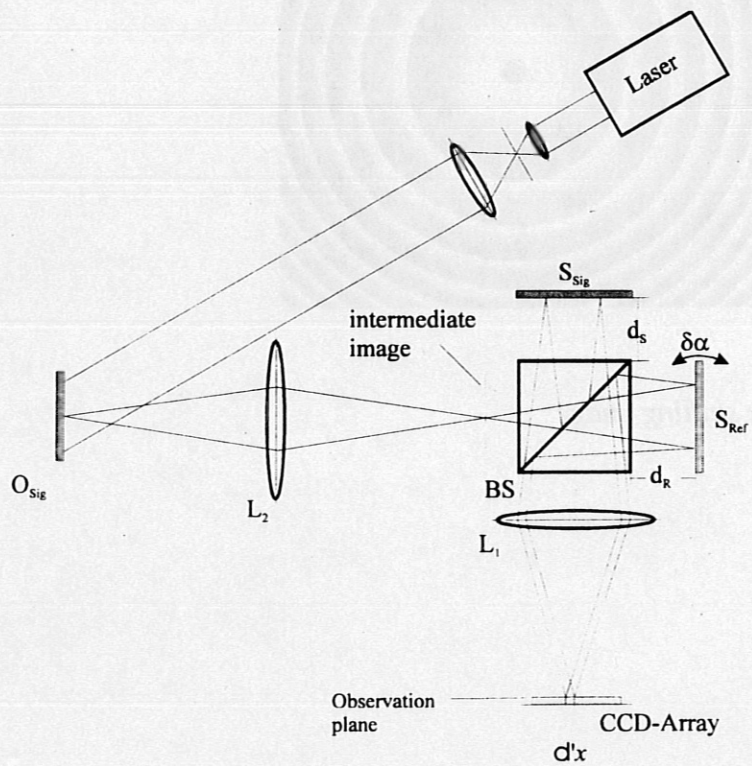

Figure 4-12: Setup of a shearing interferometer. L: lens, BS: beam splitter, S: rough surface.

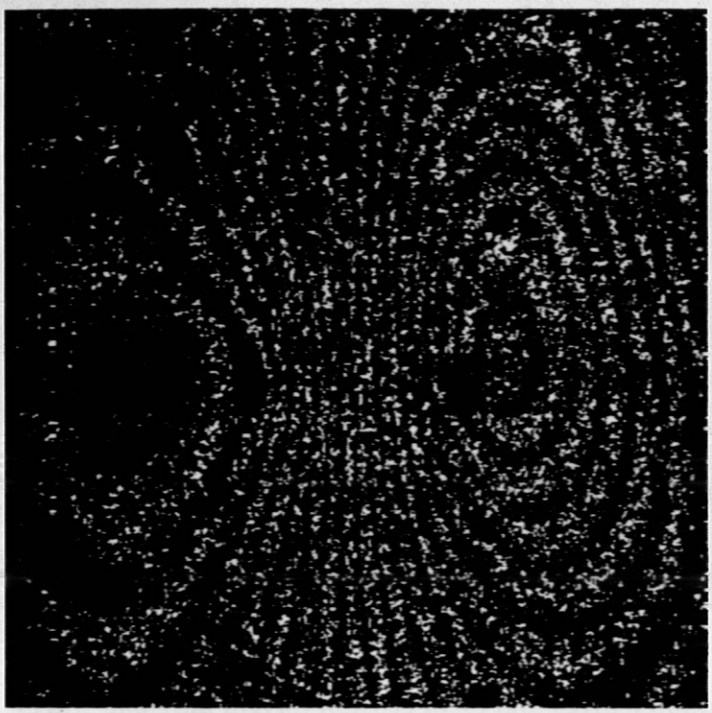

Figure 4-13: Shearing difference image of an out-of-plane deformation

All the images shown hitherto were made only with a deformation of an otherwise unchanged surface. All the experiments show good results in detecting quantitatively the change of the surface contour between two measurements.

For measurement in experimental fusion devices the discrimination between deformation and erosion/redeposition is of major concern. The next two figures (4.15-4.16) show the first attempt to achieve this aim. In the first experiment a symetrical deformation as before is combined with a local erosion. The resulting figure shows the deformation in the parts of the surface which were not eroded and clear the part of local erosion.

Figure 4-14: Deformation fringes and local erosion (bright diagonal trace)

Figure 4-15: Qualitative measurement of erosion. a) Surface before erosion, b) Surface after mechanical erosion, c) difference image from a) and b) with the location of the erosion.

List of abbreviations

ASC	angular speckle correlation
CCD	charge coupled device
MCP	micro channel plate
SSC	spectral speckle correlation

References

[1] R. Jones, C. Wykes, *Holographic and Speckle Interferometry*, Cambridge University Press, Cambridge 1989.

[2] J. C. Dainty, *Laser Speckle and Related Phenomena*, Springer, Berlin 1989.

[3] M. Fançon, *Laser Speckle and Applications in Optics*, Academic Press, New York 1979.

[4] S.A. Cohen, R.F. Mattas and K.A. Werley, Princton Plasma Physics Lab. Report PPPL-2823, (1992) (available from National Technical Information Service, Springfield, VA 22161, USA).

[5] J. Brooks, J. Nucl. Mater. 170 (1990) 164.

[6] A. W. Koch, JET Joint Undertaking Progress Report 1992 (unpublished)

[7] F. Weschenfelder, Berichte des Forschungszentrums Jülich 2793, 1993.

[8] B. de Kock, JET, Febr. 1991 (private communication).

[9] A. W. Koch, Proc. Intern. Conference on Phenomena in Ionized Gases ICPIG XX, Barga, Italy, 1991.

[10] F. Salazar, A. Trunzler, M. Ruprecht and A.W. Koch: *Measurement of Erosion and Deposition on rough surface using speckle correlation,* Rev. Scient. Instr. (in preparation)

[11] F. Salazar, LMT Laboratory Report LMT-GEN 1, 1994

[12] B. Ruffing, *Berührungslose Rauheitsmessung technischer Oberflächen mit Speckle-Korrelationsverfahren*, Ph.D. Thesis, Universität Karlsruhe (TH), 1987.

[13] J. A. Leendertz and J. N. Butters, *An image-shearing speckle-pattern interferometer for measuring bending moments*, J.Phys.E: Sci. Instrum. **6** (1973) 1107-10.

[14] W. Kirchner, *Rauheitsmessung durch Speckle Korrelation*, LMT Laboratory Report, Universität des Saarlandes, June 1994.

[15] W. Kirchner, Optische *Rauheitsmessung an technischen Oberflächen mittels Speckle Korrelation*, Diploma Thesis, LMT, Universität des Saarlandes, December 1994.

[16] D. Tutsch, *Aufbau eines Zweiwellenlängen-Interferometers mit computergestützter Bildaufnahme und Bildverarbeitung für die Speckle-Oberflächenuntersuchung*, Diploma Thesis, LMT, Universität des Saarlandes, May 1993.

[17] Th. Sinnwell, *Aufbau eines Zwei-Winkel-Speckleinterferometers zur Oberflächendiagnostik*, Diploma Thesis, LMT, Universität des Saarlandes, May 1994.

[18] A. Trunzler, *Universelle Schrittmotoransteuerung zur Automatisierung optischer Aufbauten*, LMT Laboratory Report, Universität des Saarlandes, July 1994.

[19] Chr. Wache, *Automatisierung von Laboraufbauten durch den Einsatz von Microcontroller-gesteuerten Schrittmotoren*, LMT Laboratory Report, Universität des Saarlandes, December 1994.

[20] C. Fichtner, *Bildverarbeitungsalgorithmen zur Auswertung laserinterferometrischer Oberflächenmessungen*, Diploma Thesis, LMT, Universität des Saarlandes, March 1994.

[21] G. Alt, *Realisierung einer anwenderspezifischen, hardware-orientierten Bildverarbeitung*, LMT Laboratory Report, Universität des Saarlandes, August 1994.

[22] R. Weber, Simulation von Specklemustern, Diploma Thesis, LMT, Universität des Saarlandes, September 1994.

[23] M. Ruprecht, W. Kirchner, and A.W. Koch: *Optische Rauheitsmessung an technischen Oberflächen mittels Speckle-Korrelation*, Proc. 96. Tagung der Deutschen Gesellschaft für angewandte Optik DGaO, Rügen June 1995.